Thin-film interference effects on the efficiency of a normal-incidence grating in the 100-350 Å wavelength region

J. F. Seely, L. I. Goray, W. R. Hunter, and J. C. Rife

Thin-film interference effects were observed in the normal-incidence efficiency of a 2400 groove/mm replica grating. The efficiency was measured in the 100 Å to 350 Å wavelength range and had an oscillatory behavior that resulted from the presence of a thin SiO_2 coating. The thicknesses of the SiO_2 and the underlying oxidized aluminum layers were inferred from computer modeling of the zero-order efficiency. The efficiencies in the diffracted orders were calculated using the modified integral approach and accounting for the multilayer coating and the groove profile derived from atomic force microscopy. The calculated and measured efficiencies were in good agreement.

J. F. Seely and J. C. Rife are with the Naval Research Laboratory, Washington DC 20375-5352. L. I. Goray is with I. I. G. Inc., P. O. Box 335, Penfield, New York 14526. W. R. Hunter is with SFA Inc., 1401 McCormick Drive, Landover, Maryland 20785.

14 September 1998. Submitted to Applied Optics. Revised 12 November 1998.

1. Introduction

Multilayer-coated diffraction gratings that have relatively high efficiencies at normal incidence in the extreme ultraviolet region have been developed. Peak normal-incidence efficiencies as high as 16% have been achieved.[1] The multilayer coating is matched to the groove profile so that the efficiency is optimal in a waveband of interest.

As part of the design process for the optimization of the multilayer coating and the groove profile, it is useful to have a computer program that models the efficiency of the multilayer-coated grating. The program should account for the finite conductivity of the coating, the irregular shape of the groove profile, the microroughness of the groove facets, and the two polarization orientations of the incident radiation. Such rigorous calculations demand significant computer resources, and numerical algorithms that rapidly converge are required if accurate results are to be obtained in a reasonable time.

Nevière[2,3] has adapted the differential formalism to calculate the efficiency of a multilayer grating. Calculations were presented for ideal blazed groove profiles and only for the polarization orientation with the electric field vector parallel to the grooves.

In an effort to develop a computer program that calculates grating efficiencies on a small personal computer, Goray and Chernov[4,5] have used a modified integral method. In previous work,[6] this computer program was used to model the efficiency of a 2400 groove/mm blazed grating. The calculation accounted for the groove profile as determined from atomic force microscopy (AFM), the optical properties of the SiO_2 surface, and the polarization of the incident radiation. The calculated efficiencies in the 0, ± 1, and ± 2 orders were compared to the normal-incidence efficiencies measured using

synchrotron radiation in the 125 Å to 225 Å wavelength range. The calculated and measured efficiencies of this uncoated grating were in good overall agreement.

In the present work, the measured and calculated efficiencies of a replica of the 2400 groove/mm grating that was analyzed in Ref. 6 are presented. As a result of the replication process, the grating had an oxidized aluminum surface. A thin SiO_2 overcoating was applied to the replica grating for the purpose of reducing the microroughness of the groove facets. The efficiencies in the 0, ±1, and ±2 orders, measured using synchrotron radiation, have an interesting oscillatory behavior that results from the presence of the thin SiO_2 layer on the highly reflecting oxidized aluminum surface. The thicknesses of the SiO_2 and Al_2O_3 layers were inferred from the frequency and amplitude of the zero-order efficiency in the 100 Å to 350 Å wavelength range. Using these layer thicknesses and the groove profile that was derived from AFM, the efficiencies in the 0, ±1, and ±2 orders were calculated using an enhanced version of the computer program that is based on the modified integral method[4,5] and accounts for the multilayer coating. The calculated efficiencies are in good overall agreement with the measured efficiencies. The oscillatory behavior of the efficiency as a function of wavelength, resulting from thin-film interference in the SiO_2 layer, is accurately modeled. This work demonstrates that thin-film interference effects in the efficiency of a grating with several layers can be accurately modeled on a small personal computer in a reasonable amount of time.

2. Replica Grating and Atomic Force Microscopy

The master grating was fabricated by Spectrogon UK Limited (formerly Tayside Optical Technology). The groove pattern was fabricated in fused silica using a holographic technique. The groove pattern was ion-beam etched to produce an approximately triangular, blazed groove profile. The grating has 2400 g/mm, a concave radius of curvature of 2.0 m, and a patterned area of size 45 mm by 35 mm. The master grating was uncoated.

The replica of the master grating was produced by Hyperfine, Inc. As a result of the replication process, the replica grating had an aluminum surface. A thin SiO_2 coating was applied to the aluminum surface for the purpose of reducing the microroughness.

The surface of the replica grating was characterized using a Topometrix Explorer Scanning Probe Microscope, a type of atomic force microscope (AFM). The AFM images typically had 500x500 pixels and a scan range of 1 to 20 μm (pixel size 20 to 400 Å). The silicon probe had a pyramid shape. The base of the pyramid was 3 to 6 μm in size, the height of the pyramid was 10 to 20 μm, and the height to base ratio was approximately 3. The tip of the pyramid had a radius of curvature less than 200 Å. The AFM scans were performed using the non-contact resonating mode, where the change in the oscillation amplitude of the probe is sensed by the instrument.

A surface topology reference sample was used to optimize the AFM scanning parameters, to calibrate the height scaling of the instrument, and to evaluate the performance of the AFM. This was essential for the accurate characterization of the replica grating. The surface topology reference sample consisted of an array of approximately square holes fabricated on the silicon dioxide surface of a silicon die by

VLSI Standards Inc. The top surface of the die was coated with a thin layer of platinum. The hole array had a pitch of 3 μm and a hole depth of 180 Å.

A typical image of the surface topology reference sample is shown in Fig. 1. The size of the image is 4 μm. The scan positions across the edges of the hole are indicated in Fig. 1, and the scan data across these four edges are presented in Fig. 2 (a)-(d). The corresponding line spread functions (LSF), the derivatives of the scan data, are presented in Fig. 2 (e)-(h). The widths of the LSF range from 390 to 790 Å. These four LSF are indicative of the range of LSF derived from a number of scans of the surface topology reference sample. Assuming that the sides of the holes on the sample are essentially vertical, as specified by the manufacturer, the LSF is characteristic of the probe tip size and the instrument response function. Since the LSF widths (390 to 790 Å) are 2 to 4 times the radius (≤200 Å) of the probe tip, we may conclude that the overall instrument response function is several times wider than the probe tip radius.

The power spectral densities (PSD) derived from two images of the surface topology reference sample are shown in Fig. 3. The curves labeled (a) and (b) in Fig. 3 are the PSD derived from images of size 20 and 4 μm, respectively. The rms microroughness, derived from the area under the PSD curve, is 13 Å in the frequency range 2 to 40 μm^{-1}.

In general, the measured LSF and PSD depend on the depth and the lateral pitch of the surface features and the instrumental scanning parameters. Thus it is difficult to directly transfer the information gained from the surface topology reference sample to the characterization of the replica grating. For example, the replica grating has rounded grooves with a smaller depth (85 Å) and a smaller lateral pitch (0.417 μm) compared to

the surface topology reference sample (180 Å and 3 μm, respectively). However, the surface topology reference sample was essential for calibrating the height measurements, for adjusting the instrumental scanning parameters, and for characterizing the performance of the pyramidal scanning probe.

An AFM image of two grooves of the replica grating is shown in Fig. 4. The scan was performed across the grooves over a range of 1 μm (20 Å pixels). The vertical scale in Fig. 4 has been expanded to reveal the texture of the grating surface. The PSD derived from a 2 μm size image spanning nearly 5 grooves is shown in Fig. 5. The peak in the 2 to 3 μm^{-1} frequency range results from the 0.4167 μm groove period. The rms microroughness is 7 Å in the 4-40 μm^{-1} frequency range.

By comparison, the microroughness of the master grating measured by the same type of AFM instrument was 3.2 Å,[6] and this implies that the replica grating is significantly rougher than the master grating. This may result from the replication process, which for a concave grating is at least a two step process. Furthermore, the master grating was fabricated on a fused silica surface by a holographic technique and was ion-beam polished, while the aluminum surface of the replica grating may contribute to its larger microroughness. The replica grating without the SiO_2 coating was not characterized by AFM.

A typical groove profile derived from the AFM image (1 μm in size) of the replica grating is shown in Fig. 6. The groove profile is approximately triangular in shape with rounded corners and troughs and with facet angles of 3.4^o and 6.2^o. The average groove depths derived from the AFM images are in the range 85 to 95 Å. These values of the facet angles and the groove depth are larger than the corresponding values for the

master grating, 2.5° and 5.5° facet angles and 75 Å average groove depth. Thus the grooves of the replica grating are deeper and the facet angles are steeper compared to those of the master grating.

3. Measured Efficiencies

The efficiency of the replica grating was measured using the Naval Research Laboratory beamline X24C at the National Synchrotron Light Source at the Brookhaven National Laboratory. The synchrotron radiation was dispersed by a monochromator that had a resolving power of 600.[7,8] Thin filters suppressed the radiation from the monochromator in the higher harmonics. The wavelength scale was established by the geometry of the monochromator and the absorption edges of the filters.

The replica grating was mounted in the reflectometer so that the dispersed radiation from the monochromator was incident on the grating at an angle of 15.2° measured from the normal to the surface of the grating. At fixed wavelengths, the detector was scanned in angle about the grating. Measurements were performed at 23 wavelengths in the 125-182 Å range using a silicon filter and at 17 wavelengths in the 172-225 Å range using an aluminum filter. The incident radiation was approximately 90% polarized with the electric field vector in the plane of incidence (p polarization). In this orientation, the electric field vector was perpendicular to the grating grooves.

A typical detector scan is shown in Fig. 7 for a wavelength of 187.9 Å, where the inside ($m>0$) and outside ($m<0$) diffraction orders are identified. The width of the orders

was determined primarily by the detector slit which was 0.5^o wide in the dispersion direction.

The grating was oriented so that the 3.4^o facets were facing the incident radiation. In this orientation, the inside orders were closest to satisfying the on-blaze condition for these facets, where the radiation is specularly reflected from the facets. In Fig. 7, the efficiencies in the inside orders (+1 and +2), diffracted at angles closest to the incident radiation, are more intense than the outside orders (-1 and –2). The scattered light level between the orders is low for diffraction angles in the off-blaze direction ($>15.2^o$). The scattered light level is higher in the on-blaze direction ($<15.2^o$).

The measured efficiencies were determined by fitting a background curve and five Gaussian profiles to the 0, ±1, and ±2 orders as shown by the curves in Fig. 8. The background and the five Gaussian profiles were fitted to the data points using a least squares technique. The heights of the Gaussian profiles (above the background curve) were determined for each of the 40 detector scans that were performed at fixed wavelengths in the 125-225 Å wavelength range.

While the angular positions of the diffracted orders changed with the wavelength of the incident radiation, the angular position of the zero order was fixed at an angle equal to the angle of incidence (15.2^o). The detector was positioned on the zero order, and the efficiency in the zero order was measured in the 100-138 Å range using a boron filter, in the 125-175 Å range using a silicon filter, and in the 170-340 Å range using an aluminum filter. The zero-order efficiency is shown by the data points in Fig. 9.

The zero-order efficiency, as well as the efficiencies in the diffracted orders that are discussed later, has an interesting oscillatory behavior. In contrast, the efficiency of

the uncoated master grating varied smoothly with wavelength.[6] This oscillatory behavior is attributed to the presence of the thin SiO_2 layer on the oxidized aluminum surface of the replica grating.

In order to understand the oscillatory behavior, the reflectance of a thin SiO_2 layer on an oxidized aluminum surface was calculated as a function of wavelength. The computational model consisted of an SiO_2 layer and an Al_2O_3 layer on opaque aluminum. The reflectance was calculated for an angle of incidence of 15.2^o and for p-polarized incident radiation. The wavelength positions of the extrema in the reflectance curve depended on the assumed thicknesses of the SiO_2 and Al_2O_3 layers. These two layer thicknesses were determined by matching the wavelength positions of the extrema of the calculated reflectance curve to the extrema of the measured zero-order efficiency curve of the replica grating.

Shown in Fig. 10 is the calculated reflectance of an SiO_2 layer of variable thickness and an Al_2O_3 layer of 30 Å thickness on opaque aluminum. The optical constants were derived from the compilations of Henke *et al*.[9] The three curves in Fig. 10 were calculated for the wavelengths of three of the maxima in the zero-order efficiency curve (127.5 Å, 169.0 Å, and 217.0 Å). The three curves in Fig. 10 have locally coinciding maxima at an SiO_2 thickness of 743 Å. The three curves have locally coinciding maxima for no other SiO_2 thickness. Additional calculations indicated that the local maxima in the calculated reflectance curves matched those in the measured zero-order efficiency curve only for an SiO_2 thickness of 743 ± 5 Å and an Al_2O_3 thickness of 30 ± 5 Å. In addition, the presence of the Al_2O_3 layer was necessary for the good agreement between extrema in the calculated reflectance curve and the measured zero-

order efficiency curve. The inferred thicknesses of the SiO_2 layer and the Al_2O_3 layer depend on the accuracy of the assumed optical constants.[9]

In Fig. 9, curve (b) is the calculated reflectance of the 743 Å SiO_2 layer and the 30 Å Al_2O_3 layer on opaque aluminum. The assumed angle of incidence is 15.2°, the incident radiation is 90% p-polarized, and the microroughness is 7 Å. The extrema in the calculated reflectance curve (b) in Fig. 9 and the measured zero-order efficiency curve (a) occur at the same wavelengths throughout the 100-300 Å wavelength range. The oscillations are thin-film interference features resulting from the presence of the SiO_2 coating. The oscillations diminish in amplitude at the longer wavelengths where SiO_2 is less transmissive. The wavelength resolution of the measurements, and the spectral resolution of the monochromator, were not sufficient to observe the high frequency, small amplitude oscillations at wavelengths longer than the aluminum L edge at 170 Å.

Similar calculations were performed assuming that the coating was SiO rather than SiO_2. In this case, the reflectance was lower than the measured zero-order efficiency curve at the longer wavelengths. Since the grating efficiency cannot exceed the reflectance of the coating, we infer that the composition of the coating is primarily SiO_2 rather than SiO.

The measured efficiencies in the 0, ±1, and ±2 orders as functions of the incident wavelength are shown by the curves with data points in Fig. 11. Also shown is the total efficiency which is the sum of the measured efficiencies in the five orders. The efficiencies in all of the orders have an oscillatory behavior as a function of wavelength. The period of the oscillation is the same in all orders and is related to the thicknesses of the SiO_2 and Al_2O_3 layers.

4. Calculated Efficiencies

The curves without data points in Fig. 11 are the calculated efficiencies. The efficiencies were calculated by the modified integral method[4,5] generalized for the case of a multilayer grating. Instead of expanding the groove profile in a Fourier series,[10] the actual points of the groove profile derived from AFM (Fig. 6) were used as the collocation points. This approach resulted in good convergence in the extreme ultraviolet (XUV) and x-ray wavelength regions and improved accuracy for calculations using an arbitrary groove profile. In addition, instead of the usual representation of the Green functions and their derivatives as Hankel functions, expansions along the exponential function series were used. This resulted in a higher accuracy of the solution and shorter calculation times.

Very fast convergence was achieved for the case of a multilayer grating with a non-ideal, arbitrary groove profile operating in the XUV and x-ray wavelength regions. These results were realized notwithstanding the fact that the spacing between the collocation points was equivalent to less than one, or in some cases a few, wavelengths of the radiation.

The computer program, written in the C^{++} language, implements several mathematical and programming improvements. For the purpose of using the computer memory more economically for the case of large numbers of collocation points and layers, the matrices are inverted along one row. The calculation of the real and imaginary parts of the complex variables, relating particularly to the exponential functions, are

carried out separately from each other. The complicated mathematical functions are coded with the Assembler programming language.

For 210 collocation points (the dimension of the square matrix), the calculation of the multilayer grating efficiency for one wavelength required only 128 seconds on a rather small personal computer (133 MHz Pentium with 64 Mbyte RAM). Typically only several Mbytes of RAM were actually used.

The calculation of the multilayer grating efficiency was performed for wavelengths in the 125-225 Å range and for an angle of incidence of 15.2^{o} (with respect to the normal to the grating surface). The grating facets were oriented identically to that during the measurements, with the shallower facet (blaze angle 3.4^{o}) facing the incident radiation. The electric field vector was perpendicular to the grooves. The surface layers were specified to be an SiO_2 layer of thickness 743 Å and an Al_2O_3 layer of thickness 30 Å on opaque aluminum. The 0, ±1, ±2, ±3, ±4, and ±5 orders were included in the calculation. The efficiencies of the orders higher than $|3|$ were quite low.

As shown by the curves without data points in Fig. 11, the calculated efficiencies have the same oscillatory behavior as the measured values. The calculated and measured efficiencies in the ±1 orders are in excellent agreement, while for the ±2 orders the calculated efficiencies tend to be higher than measured. The zero-order calculated efficiency is also higher than measured for the shorter wavelengths. Considering that there are no free parameters in the calculation of the efficiencies, the overall agreement between the calculated and measured efficiencies is considered to be remarkably good.

The explanation of the differences between the calculated and measured efficiencies will require additional studies that are beyond the scope of the present work.

These differences may result from an incomplete modeling of the microroughness of the groove profile and variations in the groove depth with spatial periods larger than the groove spacing that are not accounted for in the present calculation. It is possible that the microroughness of the SiO_2 layer, the oxidized aluminum layer, and the grating substrate may be different, and this was not accounted for in the computational model.

The measured and calculated efficiencies are shown in Figs. 12 (a) and (b), respectively. These plots reveal the relationship of the efficiencies in the various orders as functions of wavelength. For example, the +1 efficiency is highest at the longer wavelengths, while the +2 order is highest at the shorter wavelengths. This is consistent with the blaze condition $m\lambda = 2d \sin\varphi \sin\theta$, where d is the groove spacing, φ is the blaze angle, and θ is the grazing angle on the facet.[11] In Fig. 12, the measured and calculated efficiencies in the -1 and +2 orders cross at wavelengths of 204 Å and 210 Å, respectively. The measured and calculated efficiencies in the +1 and +2 orders cross at wavelengths of 162 Å and 182 Å, respectively.

The groove profile used in the calculation (Fig. 6) has an average peak to valley depth of 85 Å. By performing calculations using the same groove profile but scaled to different assumed groove depths, it was found that the wavelengths of the crossings of the –1 and +2 orders and of the +1 and +2 orders were very sensitive to the assumed groove depth. For example, the +1 and +2 crossing occurred at wavelengths of 152 Å, 182 Å, and 203 Å for assumed groove depths of 75 Å, 85 Å, and 95 Å.

In general, the calculated efficiencies in the +1 and –1 orders tend to decrease with increasing groove depth. This is illustrated in Fig. 13 for the +1 order. As the groove depth increases, the calculated efficiencies in the +2 and –2 orders increase at the longer

wavelengths and decrease at the shorter wavelengths. These trends are consistent with the blaze condition, where the blaze angle φ and the blaze wavelength mλ increase with groove depth. The best overall agreement between the calculated and measured efficiencies was achieved with an average peak to valley groove depth of 85 Å as shown in Fig. 6.

5. Conclusions

The oscillatory behavior (as a function of wavelength) of the measured normal-incidence efficiency of a replica grating was identified as a thin-film interference effect resulting from the presence of a thin SiO_2 layer on a highly-reflecting oxidized aluminum surface. The SiO_2 and Al_2O_3 layer thicknesses were inferred from the wavelengths of the extrema of the measured zero-order efficiency.

The modified integral method described in Refs. 4 and 5 was extended to accurately calculate the efficiency of the multilayer-coated grating in the soft x-ray region. The calculation used a realistic groove profile derived from the AFM images and accounted for the rounding of the corners of the groove profile and the microroughness of the facets. The thicknesses of the SiO_2 and Al_2O_3 layers, on the opaque aluminum layer, that were used in the calculation were those independently derived from the oscillations in the measured zero-order efficiency. Thus there were no free parameters in the calculation, and the comparison of the calculated and measured efficiencies was a severe test of the validity of the computational modeling.

The calculated and measured efficiencies in the +1 and –1 orders were in excellent agreement. The calculated efficiencies in the +2 and –2 orders tended to be larger than measured.

The wavelengths of the crossings of the efficiency curves were sensitive functions of the assumed groove depth, and this constrained the computational model and further tested its validity. The wavelength crossings of the calculated and measured efficiencies were in good agreement for an average peak to valley groove depth of 85 Å that was consistent with the AFM characterization of the grating surface.

The efficiency calculations were performed on a small personal computer. Considering the good overall agreement between the calculated and measured efficiencies and the reasonable computation time on a small computer, the modified integral method appears to be a useful tool for the design of multilayer gratings.

Acknowledgments

This work was supported by NASA project W19193. Part of the work was done at the National Synchrotron Light Source, which is sponsored by the Department of Energy under contract DEAC02-76CH00016. The atomic force microscope images were recorded in collaboration with Dr. Kaj Stolt of Analytical Answers Inc. We thank B. Bach of Hyperfine Inc. for information concerning the replication of the grating.

References

1. J. F. Seely, M. P. Kowalski, R. G. Cruddace, K. F. Heidemann, U. Heinzmann, U. Kleineberg, K. Osterried, D. Menke, J. C. Rife, and W. R. Hunter, "Multilayer-coated laminar grating with 16% normal-incidence efficiency in the 150 Å wavelength region," Appl. Opt. **36**, 8206-8213 (1997).
2. M. Nevière, "Multilayer coated gratings for x-ray diffraction: differential theory," J. Opt. Soc. Am. A **8**, 1468-1473 (1991).
3. M. Nevière, "Bragg-Fresnel multilayer gratings: electromagnetic theory," J. Opt. Soc. Am. A **11**, 1835-1845 (1994).
4. L. I. Goray, "Numerical analysis for relief gratings working in the soft x-ray and XUV region by the integral equation method," in *X-Ray and UV Detectors*, edited by R. B. Hoover and M. W. Tate, S.P.I.E vol. **2278**, 168-172 (1994).
5. L. I. Goray and B. C. Chernov, "Comparison of rigorous methods for x-ray and XUV grating diffraction analysis," in *X-Ray and Extreme Ultraviolet Optics*, edited by R. B. Hoover and A. B. C. Walker, S.P.I.E vol. **2515**, 240-245 (1995).
6. M. P. Kowalski, J. F. Seely, L. I. Goray, W. R. Hunter, and J. C. Rife, "Comparison of the calculated and the measured efficiencies of a normal-incidence grating in the 125-225 Å wavelength range," Appl. Opt. **36**, 8939-8943 (1997).
7. J. C. Rife, H. R. Sadeghi, and W. R. Hunter, "Upgrades and recent performance of the grating/crystal monochromator," Rev. Sci. Instrum. **60**, 2064-2067 (1989).
8. W. R. Hunter and J. C. Rife, "An ultrahigh vacuum reflectometer/goniometer for use with synchrotron radiation," Nucl. Instrum. Methods **A246**, 465-468 (1986).

9. B. L. Henke, E. M. Gullikson, and J. C. Davis, “X-ray interactions: photoabsorption, scattering, transmission, and reflection at E=50-30,000 eV, Z=1-92,” At. Data Nucl. Data Tables **54**, 181-342 (1993). Updated optical constants were obtained from the internet site cindy.lbl.gov/optical_constants.
10. D. Meystre, “A new general integral theory for dielectric coated gratings,” JOSA **68**, 490-495 (1978).
11. J. F. Seely, M. P. Kowalski, W. R. Hunter, J. C. Rife, T. W. Barbee, Jr., G. E. Holland, C. N. Boyer, and C. M. Brown, “On-blaze operation of a Mo/Si multilayer-coated, concave diffraction grating in the 136-142 Å wavelength region and near normal incidence,” Appl. Opt. **32**, 4890-4897 (1993).

Figure Captions

Fig. 1. The AFM image of the surface topology reference sample. The image size is 4 μm. The scan positions across the edges of the hole are indicated.

Fig. 2. (a)-(d) The AFM scan data across the edges of a hole on the surface topology reference sample. (e)-(h) The line spread functions.

Fig. 3. The PSD of the surface topology reference sample derived from AFM images of sizes (a) 20 μm and (b) 4 μm.

Fig. 4. AFM image of 2 grooves the 2400 g/mm replica grating. The image size is 1 μm by 1 μm. The horizontal and vertical scales are indicated.

Fig. 5. The PSD of the 2400 g/mm replica grating derived from an AFM image of size 2 μm.

Fig. 6. A typical groove profile derived from the AFM image of the 2400 g/mm replica grating. The average peak to valley groove depth is 85 Å. The blaze angles, measured from the horizontal, of the left and right facets are 3.4^{o} and 6.2^{o}, respectively.

Fig. 7. The measured grating efficiency, as a function of the diffraction angle, for a wavelength of 187.9 Å and an angle of incidence of 15.2°. The inside (m>0) and outside (m<0) diffraction orders are indicated.

Fig. 8. The fit of Gaussian profiles (smooth curves) to the measured grating efficiencies (data points). The wavelength of the incident radiation was 187.9 Å, and the angle of incidence was 15.2°.

Fig. 9. (a) The measured grating efficiency in the zero order at an angle of incidence of 15.2°. (b) The reflectance of 743 Å of SiO_2 and 30 Å of Al_2O_3 on opaque aluminum calculated at an angle of incidence of 15.2°.

Fig. 10. The calculated reflectance of a layer of SiO_2 of variable thickness and a 30 Å layer of Al_2O_3 on opaque aluminum for the three wavelengths (a) 217.0 Å, (b) 169.0 Å, and (c) 127.5 Å. The vertical dashed line indicates the only SiO_2 thickness (743 Å) at which the maxima of the three reflectance curves coincide.

Fig. 11. Comparison of the measured grating efficiency (data points) and the calculated efficiency (curves without data points) for the diffraction orders (a) +1, (b) +2, (c) –1, (d) –2, (e) 0, and (f) sum of all orders.

Fig. 12. (a) The measured and (b) the calculated grating efficiencies in the indicated orders.

Fig. 13. The efficiency in the +1 order calculated for assumed groove depths of 75 Å, 85 Å, and 95 Å. The measured +1 order efficiency is shown by the data points.

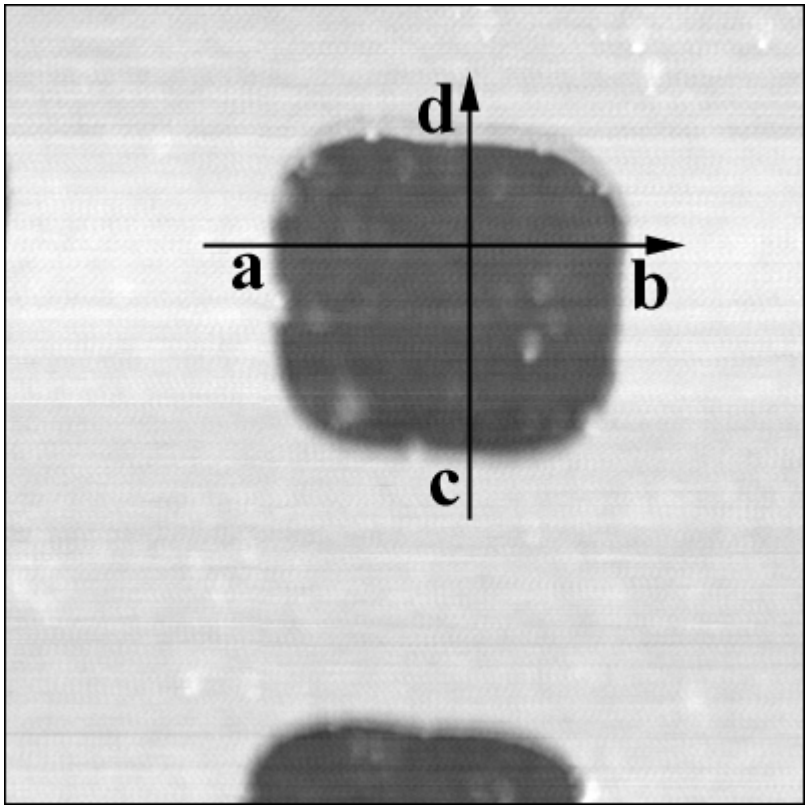

Figure 1 Seely *et al.*

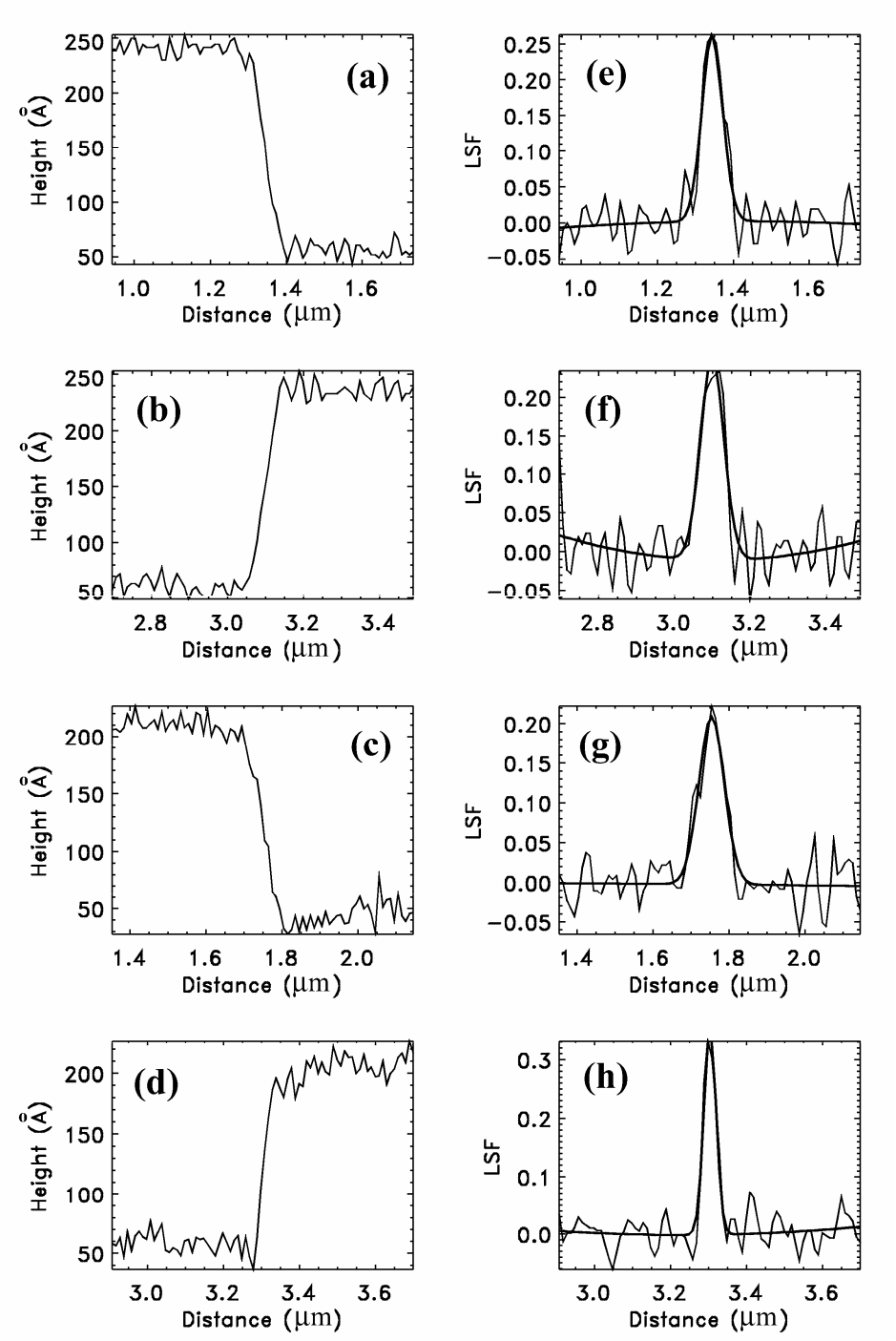

Figure 2 Seely *et al.*

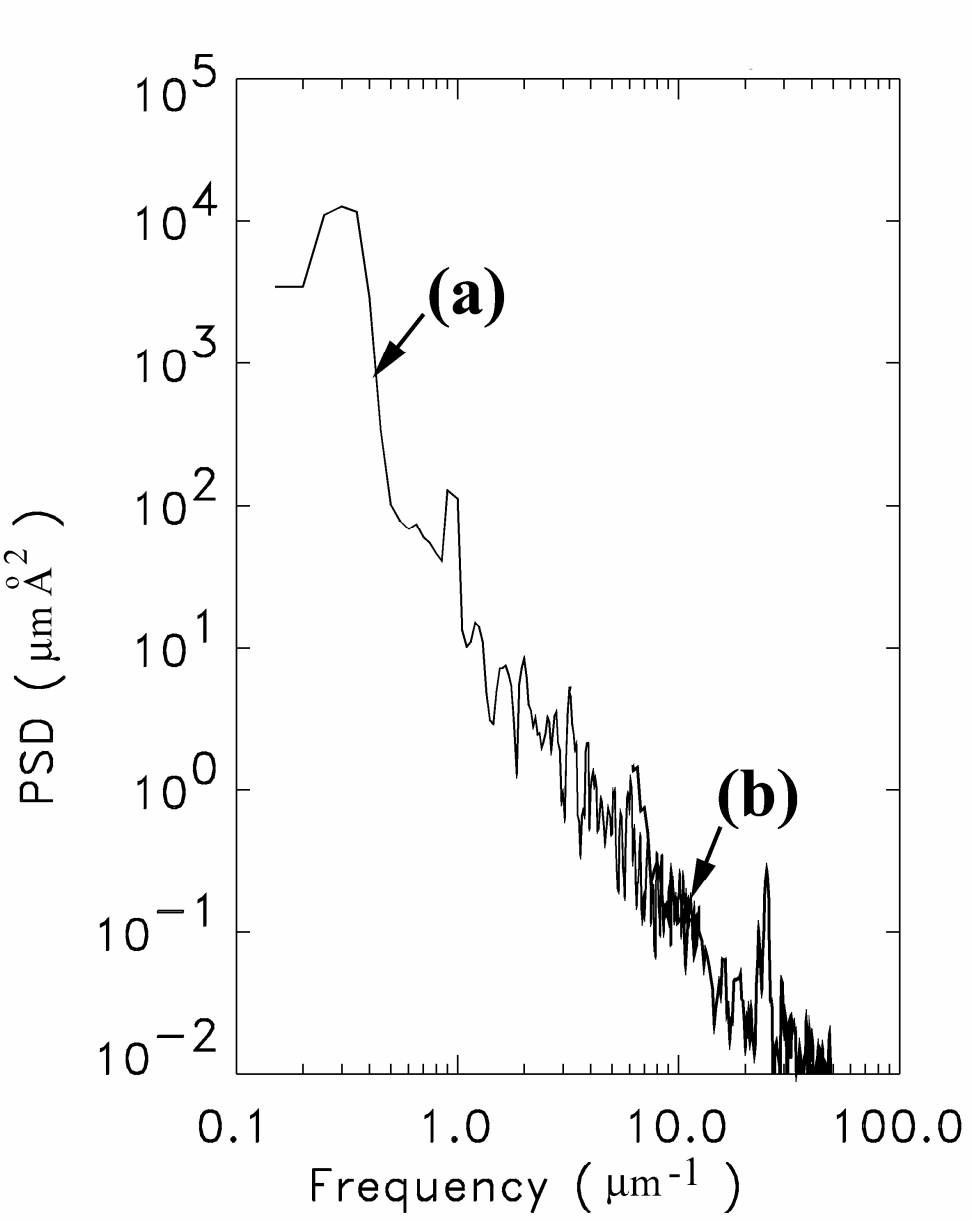

Figure 3 Seely *et al.*

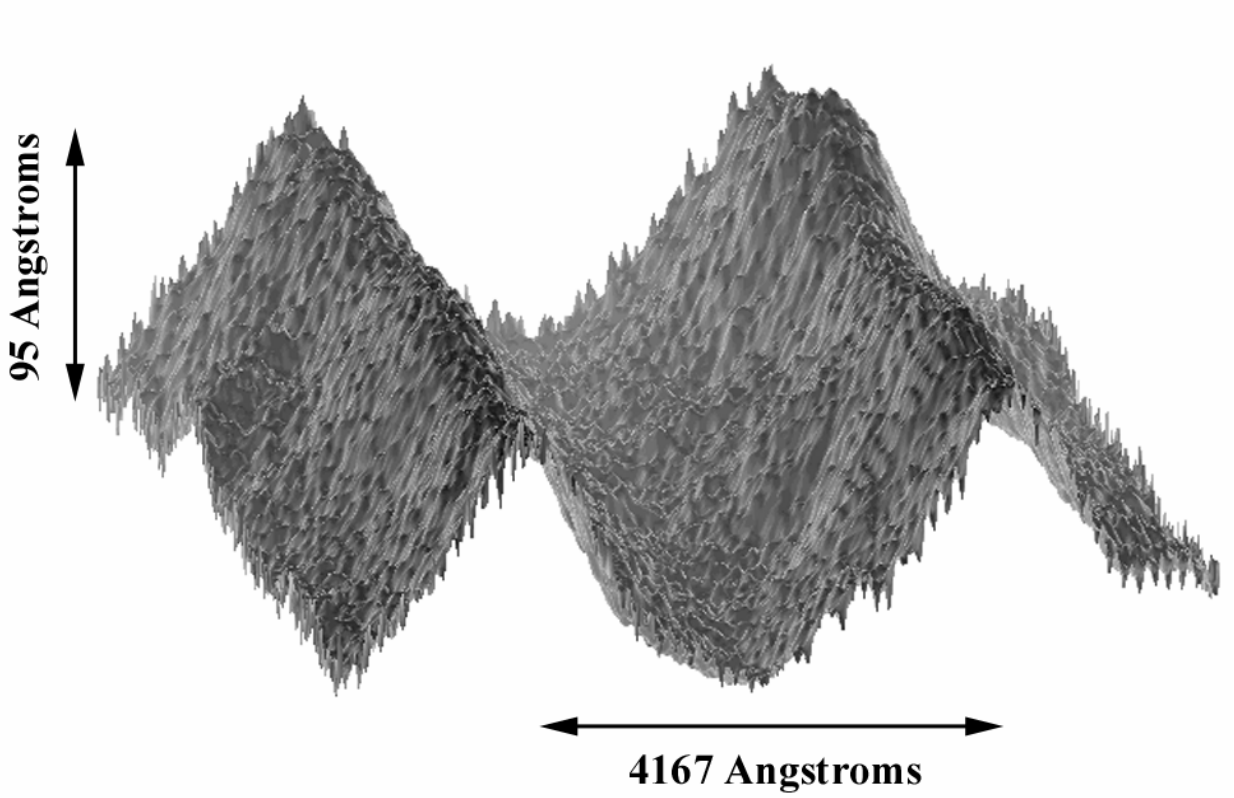

Figure 4 Seely *et al.*

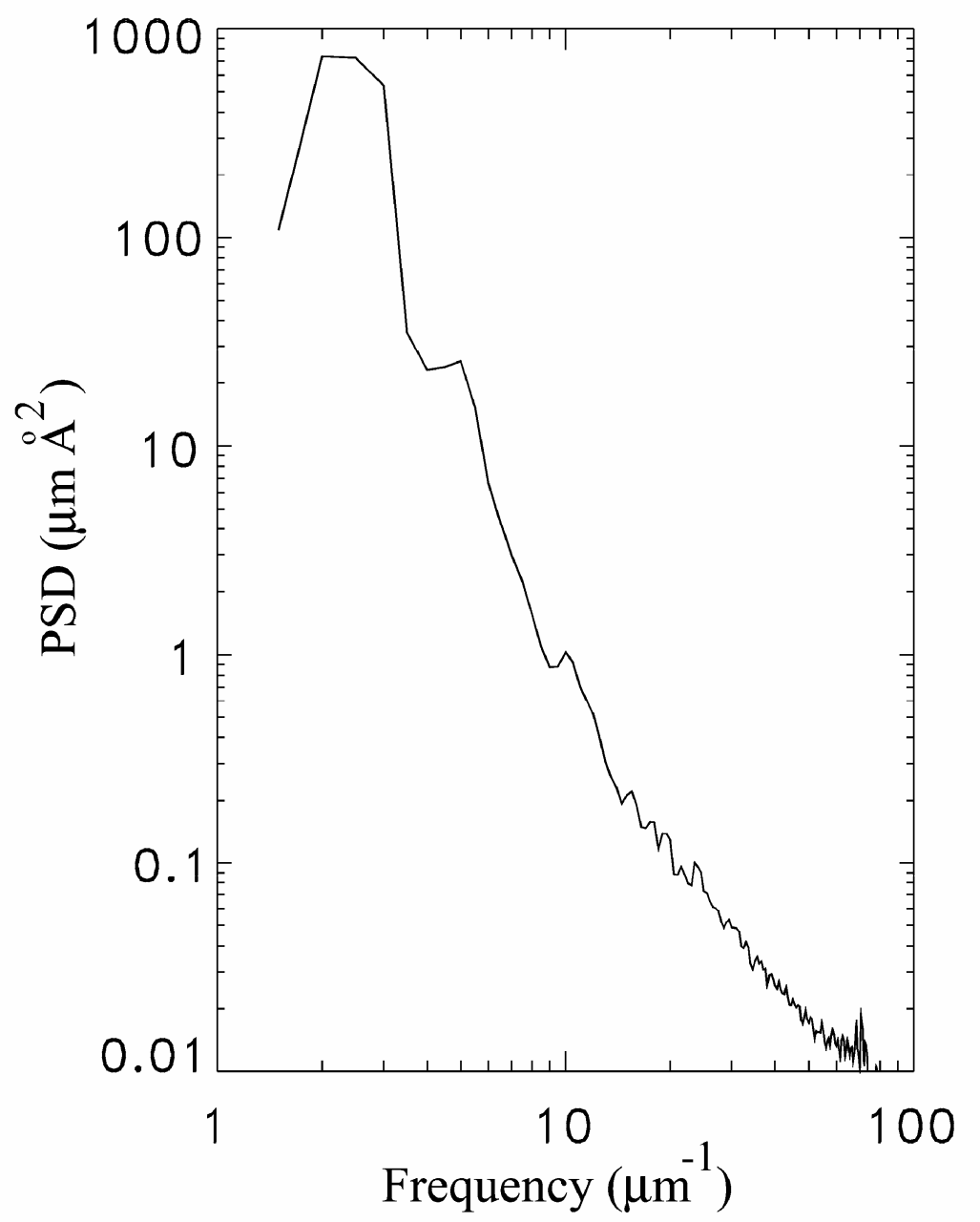

Figure 5 Seely *et al.*

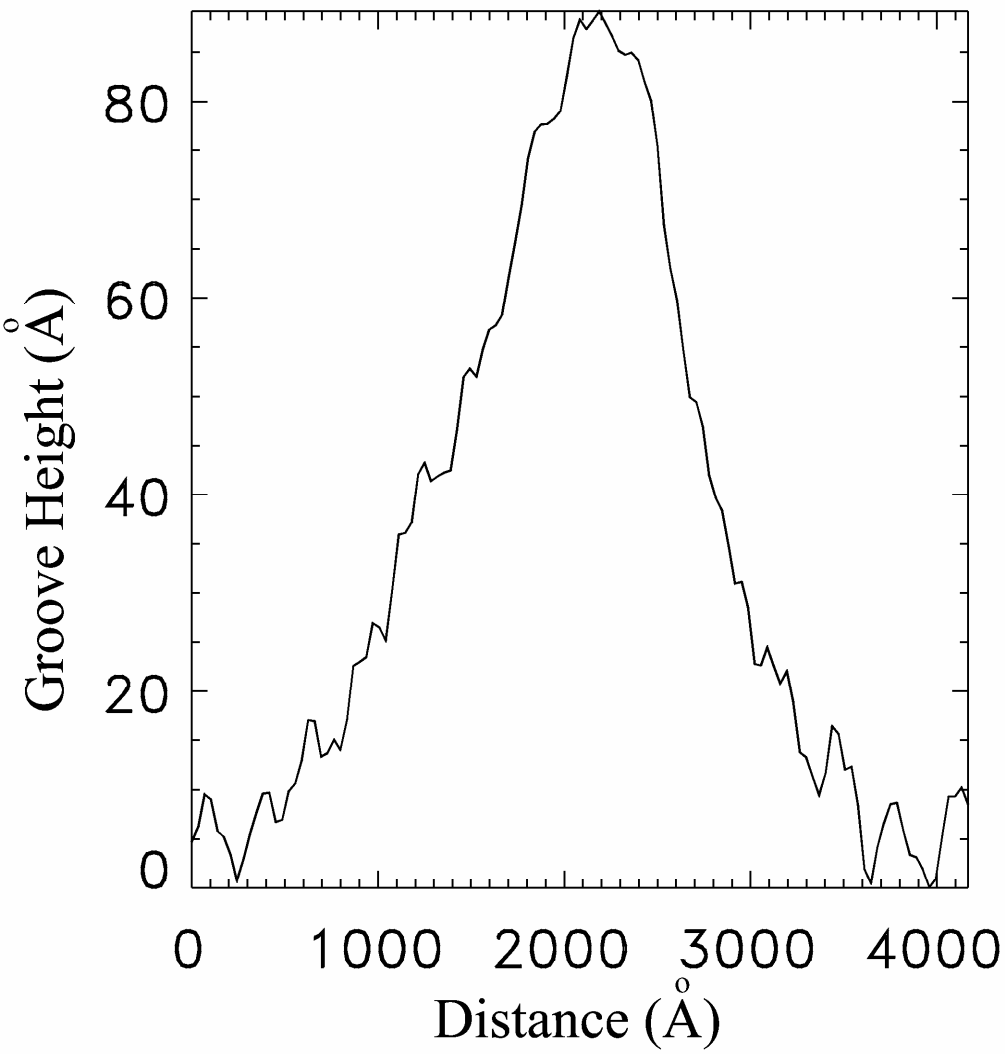

Figure 6 Seely *et al.*

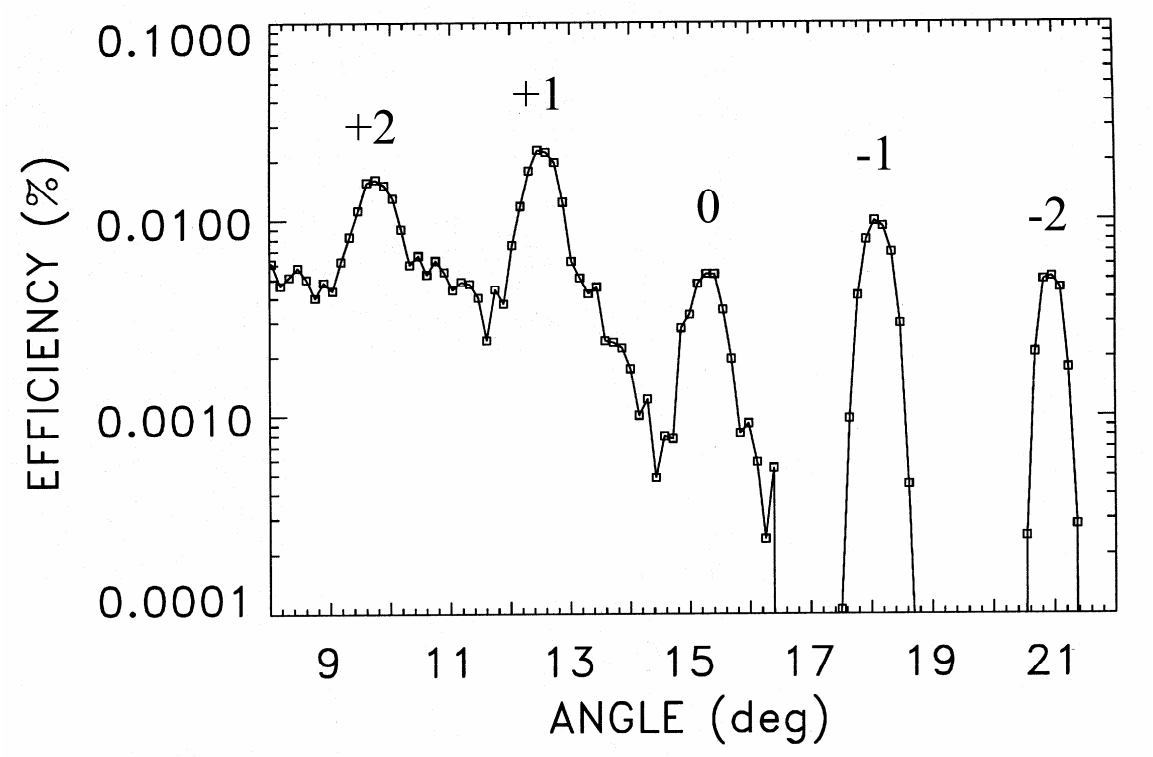

Figure 7 Seely *et al.*

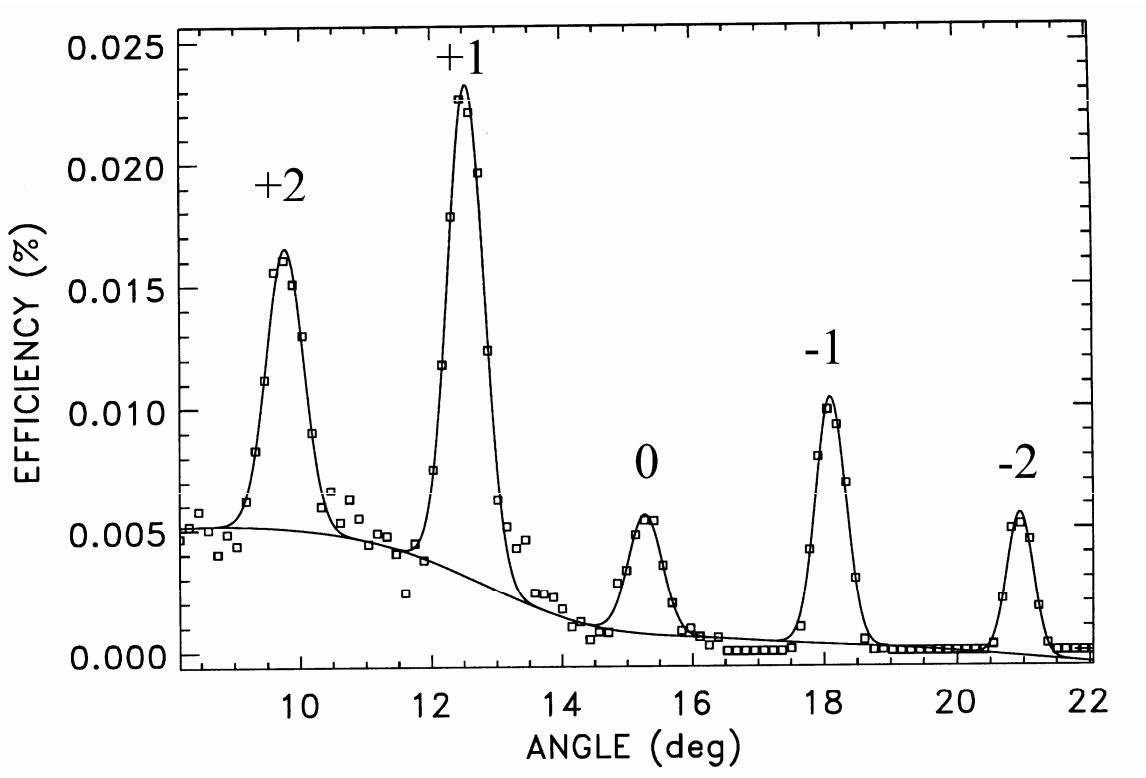

Figure 8 Seely *et al.*

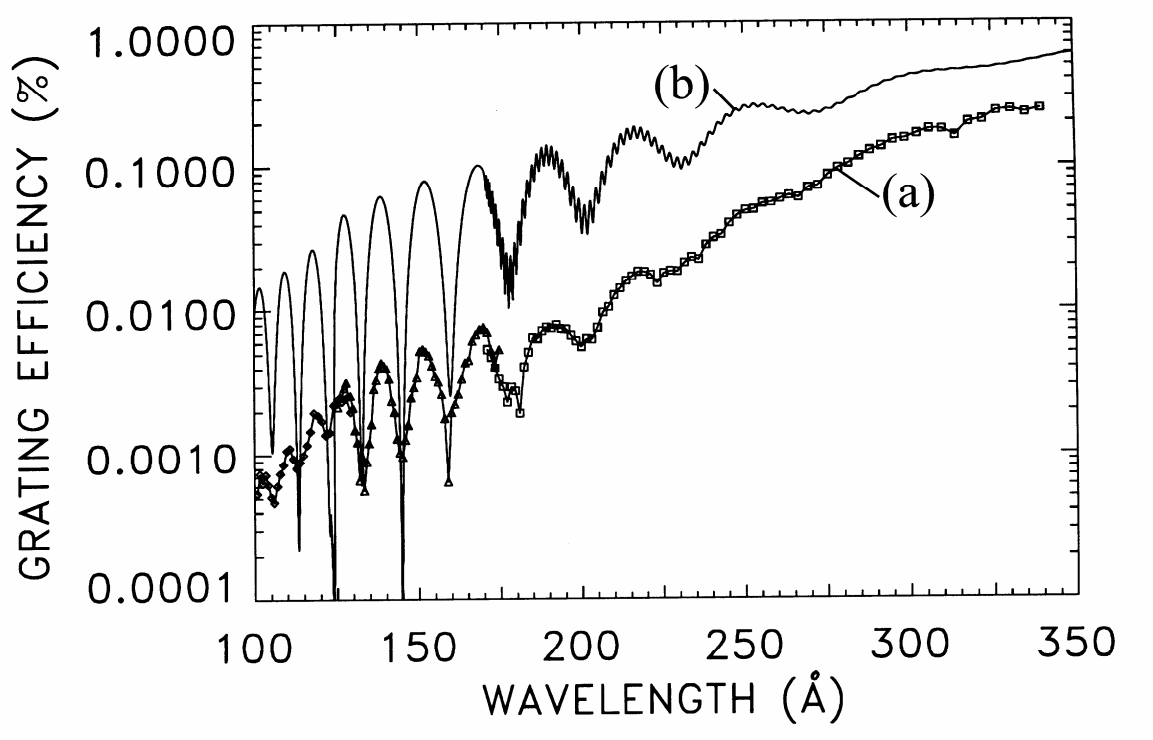

Figure 9 Seely *et al.*

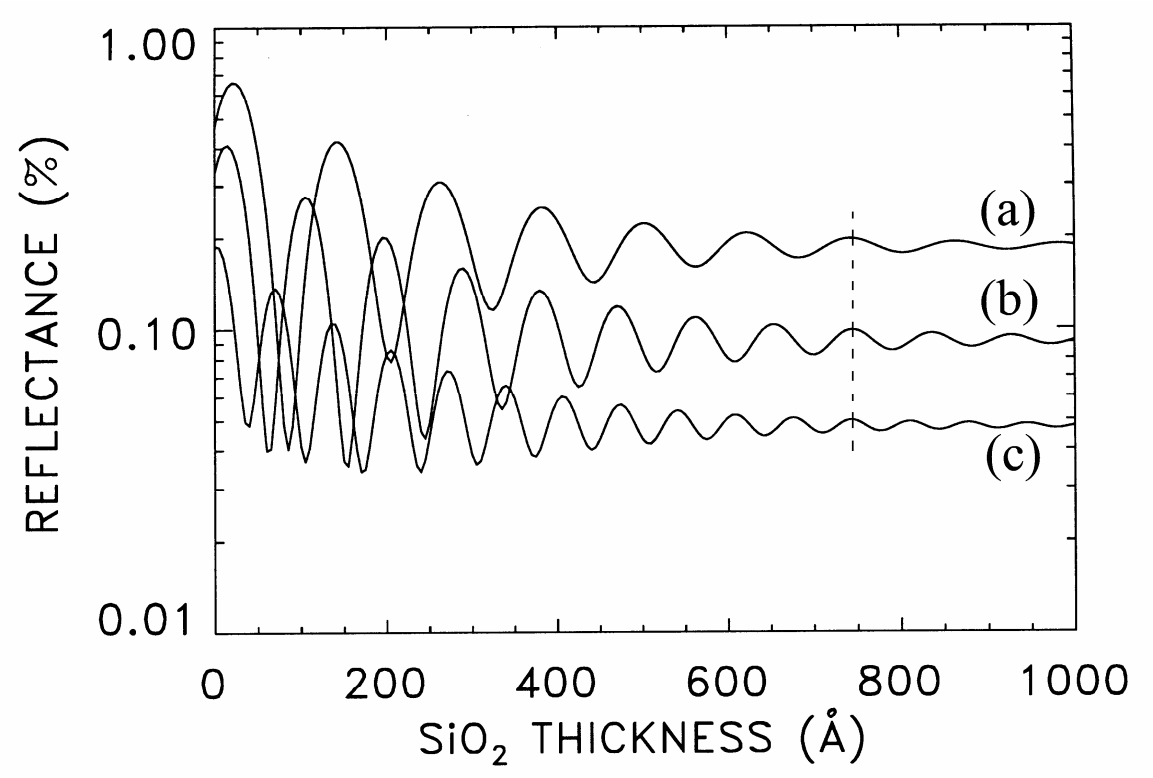

Figure 10 Seely *et al.*

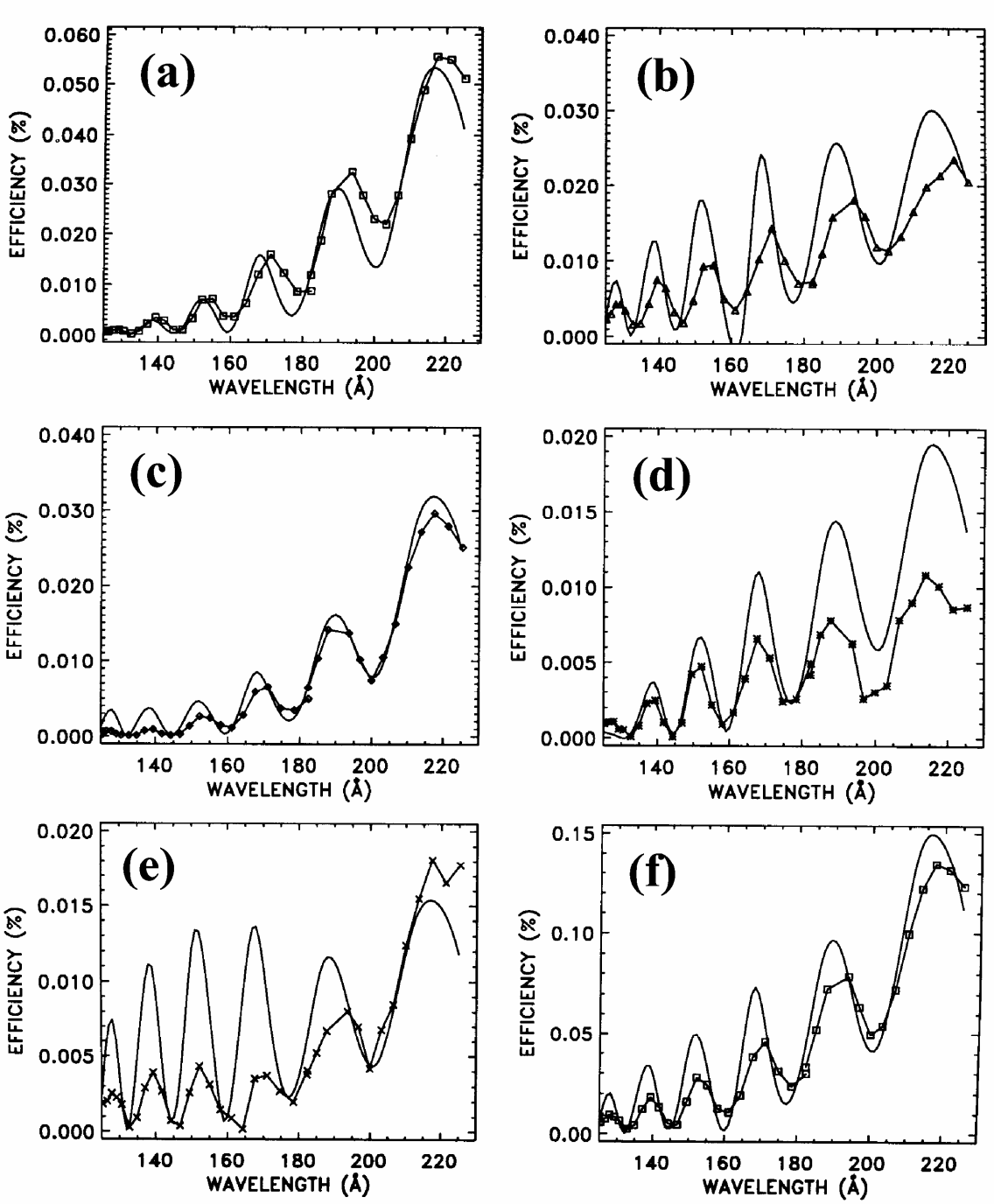

Figure 11 Seely *et al.*

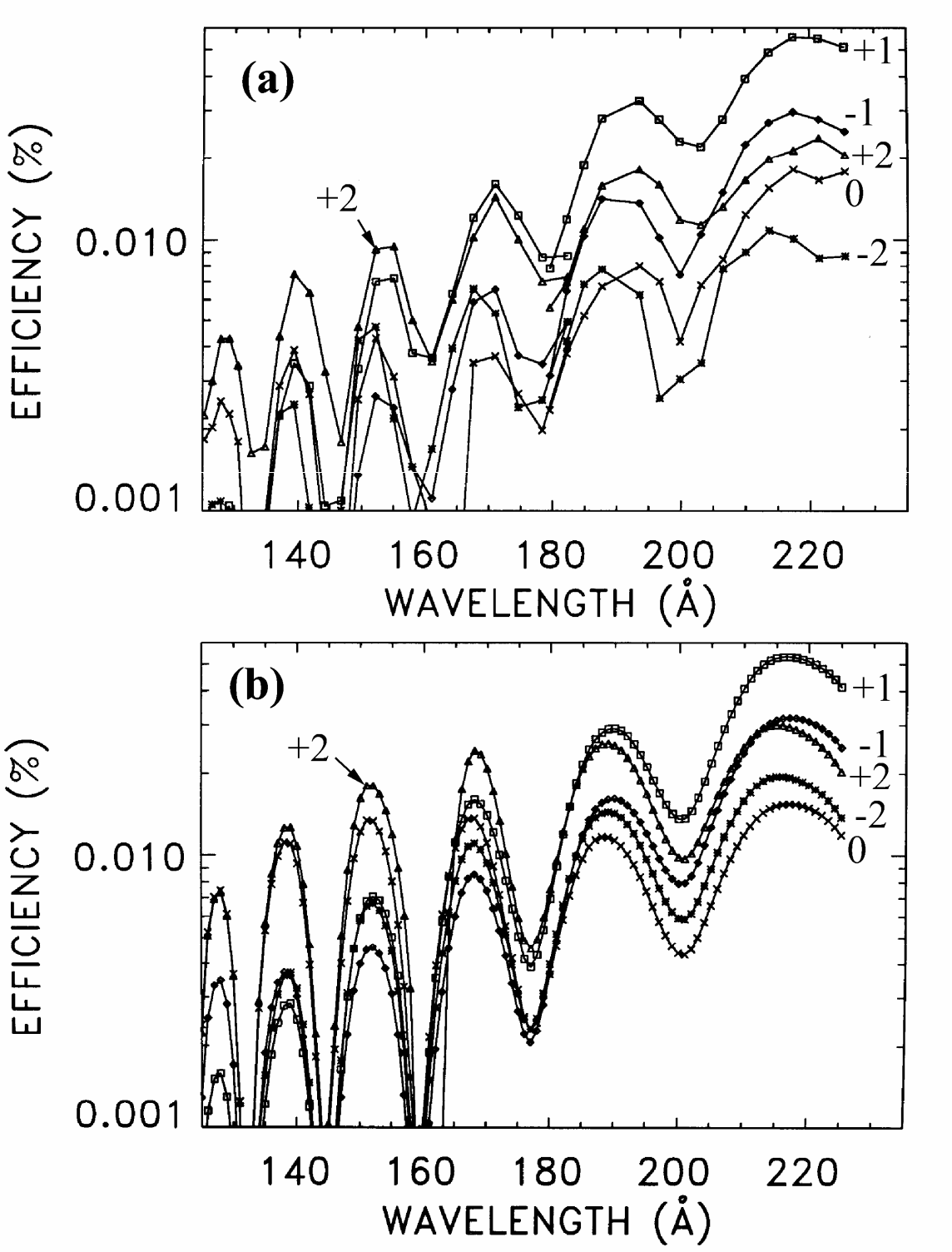

Figure 12 Seely *et al.*

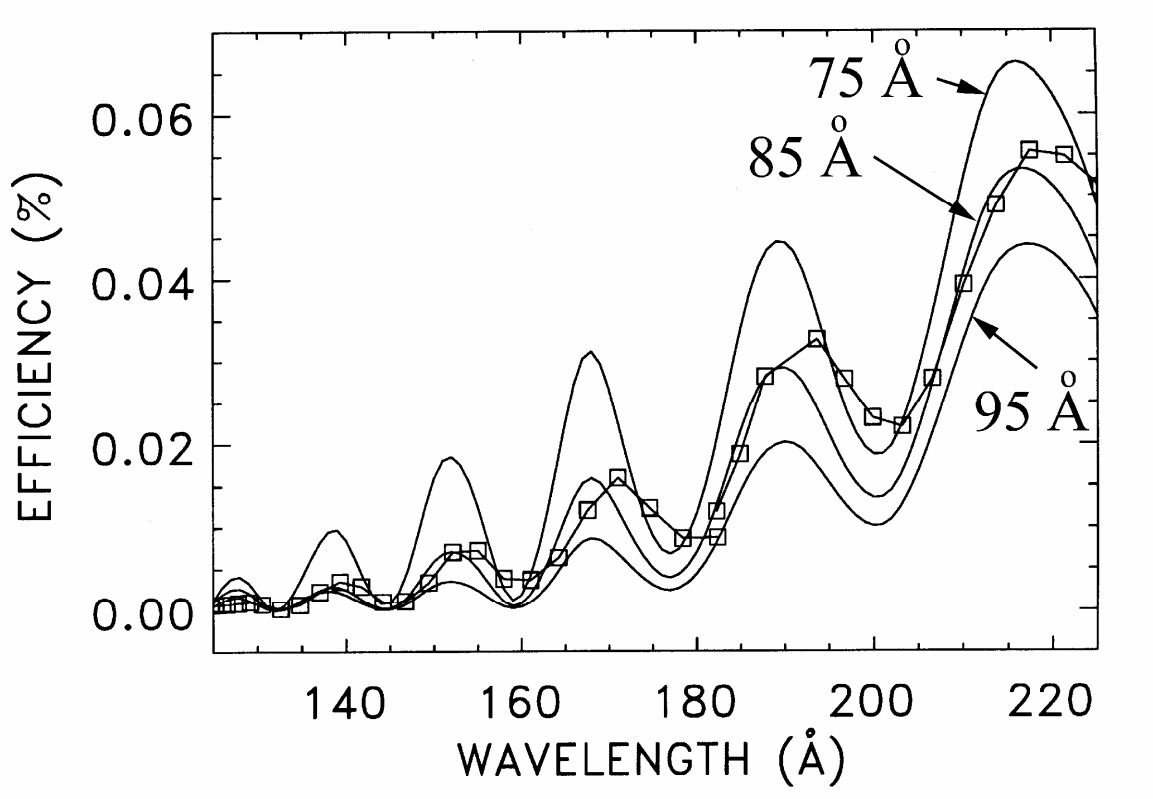

Figure 13 Seely *et al.*